

Leakage Current Reduction in VLSI Systems

David Blaauw, Steve Martin, *Krisztian Flautner, Trevor Mudge

University of Michigan, Ann Arbor, MI

*ARM Ltd, Cambridge, UK

Abstract

There is a growing need to analyze and optimize the stand-by component of power in digital circuits designed for portable and battery-powered applications. Since these circuits remain in stand-by (or sleep) mode significantly longer than in active mode, their stand-by current, and not their active switching current, determines their battery life. Hence, stringent specifications are being placed on the stand-by (or leakage) current drawn by such devices. As the power supply voltage is reduced, the threshold voltage of transistors is scaled down to maintain a constant switching speed. Since reducing the threshold voltage increases the leakage of a device exponentially, leakage current has become a dominant factor in the design of VLSI circuits. In this paper, we describe a method that uses simultaneous dynamic voltage scaling (DVS) and adaptive body biasing (ABB) to reduce the total power consumption of a processor under dynamic computational workloads. Analytical models of the leakage current, dynamic power, and frequency as a function of supply voltage and body bias are derived and verified with SPICE simulation. Given these models, we show how to derive an analytical expression for the optimal trade-off between supply voltage and body bias, given a required clock frequency and duration of operation. The proposed method is then applied to a processor and is compared with DVS alone for workloads obtained using real-time monitoring of processor utilization for four typical applications.

1. Introduction

Power consumption has become an overriding constraint for microprocessor designs, not only in mobile environments, but in desktop and server applications as well. Traditionally, the supply voltage of microprocessors has been set at the maximum allowable voltage based on device breakdown potentials, and the processor is run at maximum clock frequency. During typical use, however, the dynamic load of applications running on a processor results in substantial periods of operation where the maximum performance of the processor is not required. A number of methods have been proposed that take advantage of these periods of low utilization by scaling the supply voltage and clock frequency, resulting in a reduction in dynamic power consumption [1-3].

While these dynamic voltage scaling (DVS) methods are effective in addressing the dynamic power consumption, they are not as effective in reducing the leakage or static power. As minimum feature size continues to shrink, the scaling of the maximum supply voltage requires a reduction in the threshold voltage which results in an exponential increase of leakage current with each new technology generation. Even in today's technologies, it is not uncommon for leakage power to comprise as much as 20% of the total power consumption [4]. As technologies continue to scale, it is expected that leakage power consumption will become comparable to dynamic power consumption [5]. Furthermore, during periods of low utilization, the lower clock frequency and lower corresponding voltage level result in reduced dynamic power consumption, thereby causing leakage power to dominant.

For processors operating under dynamic computational loads, it is therefore essential that both leakage and dynamic power are addressed effectively. Previously, adaptive reverse body biasing (ABB) has been proposed to control the leakage current during standby mode [6-8]. Recently, methods using forward body biasing have also been proposed [9,10]. Adaptive body biasing has the advantage that it reduces the leakage current exponentially, whereas dynamic voltage scaling reduces leakage current linearly. In this paper, we propose the use of simultaneous dynamic voltage scaling and adaptive reverse body biasing to control both dynamic and leakage power.

The difficulty in employing simultaneous DVS and ABB is in determining the optimal trade-off between supply voltage and reverse body bias voltage, such that the total power consumption at a particular frequency of operation is minimized. The optimal trade-off between supply voltage and body voltage depends on the frequency of operation, since this determines the relative magnitude of the dynamic and static power consumption. The energy required for switching the supply voltage and the body voltage is amortized over the period of operation at a particular frequency. Since the switching energy for the body voltage and supply voltage differ, the optimal trade-off therefore also depends on the length of the operation at a particular frequency. Finally, the possible combinations of supply voltage and body-bias are constrained by the requirement that the circuit delay meets the specified clock frequency.

In this paper, we derive an analytical expression for the optimal supply voltage and body voltage for a given processor frequency and duration of operation. We present analytical models that express the power consumption and processor performance as a function of the body voltage and supply voltage and show how to fit these functions to SPICE simulation results with good accuracy. By using the performance of the processor as a constraint, the resulting two dimensional optimization task is reduced to a one dimensional task and is solved through differentiation. The analytical expression for the optimal supply voltage and body bias was verified through SPICE simulations.

The proposed simultaneous DVS and ABB method was then applied to a processor and was compared with using DVS alone. The dynamic processor loads were obtained through measurements on a 600MHz Crusoe processor for four different applications. Expected gains from using simultaneous DVS and ABB were evaluated at a current 0.18 μ m technology as well as for a projected 0.07 μ m technology. The simulations show that the proposed method improves the total power consumption by an average of 23% for the 0.18 μ m process and by an average of 49% for the 0.07 μ m process. These substantial savings in total power result from the fact that for many applications, the processor spends substantial periods of time at very low performance levels where leakage current dominates the total power consumption. The results also indicate that for future technologies with higher leakage power, the effectiveness of the proposed method will increase.

The remainder of this paper is organized as follows. In Section 2, the models for dynamic power, leakage power, and performance as a function of supply voltage and body bias are presented. In Section 3, we derive the optimal trade-off point for the supply voltage and body bias. In Section 4 we apply these optimization techniques to the Crusoe processor and in Section 5 we draw our conclusions.

2. Power and Performance Models

We first derive the threshold voltage as function of the supply and bias voltages and then express the total power consumption as function of these voltages. We then derive the performance as a function of the supply and body bias voltage. In all cases, we compare the analytical model to SPICE simulation results.

2.1 Threshold Voltage

The threshold voltage of a short-channel MOSFET transistor in the BSIM model [11,12] is given by,

$$V_{th} = V_{th0} + \gamma(\sqrt{\Phi_s - V_{bs}} - \sqrt{\Phi_s}) + \Delta V_{SCE} + \Delta V_{NW} \quad (1)$$

where V_{th0} is the zero-bias threshold voltage, Φ_s and γ are constants for a given technology, V_{bs} is the voltage applied between the body and source of the transistor, ΔV_{sce} is the dependence of the threshold voltage on short channel effects and drain induced barrier lowering, and ΔV_{NW} is a constant for a given transistor size that models narrow width effects. The change in threshold voltage due to short channel effects is given by,

$$\Delta V_{SCE} \approx -\theta(SCE) - \theta(DIBL) \cdot V_{dd} \quad (2)$$

where $\theta(DIBL)$ is a function dependent only on process dependent fitting parameters and effective length of the transistor, $\theta(SCE)$ is approximately a constant, and V_{dd} is the supply voltage. Combining (1) and (2) shows that V_{th} has a linear dependence with V_{dd} . If $|V_{bs}| \approx \Phi_s$ then $\sqrt{\Phi_s - V_{bs}} - \sqrt{\Phi_s}$ can be linearized as $k \cdot V_{bs}$ which yields,

$$V_{th} = V_{th1} - K_1 \cdot V_{dd} - K_2 \cdot V_{bs} \quad (3)$$

where K_1 , K_2 and V_{th1} are constant fitting parameters. Figure 1 shows the linear dependence of V_{th} versus V_{dd} and V_{bs} as given by SPICE simulation of the Berkeley predictive models for a 0.07 μ m process [13]. A least squares method linear regression of V_{th} vs. V_{dd} and V_{bs} matches with (3) with a regression coefficient, R^2 , of 0.997, where an R^2 value of 1 is a perfect linear fit.

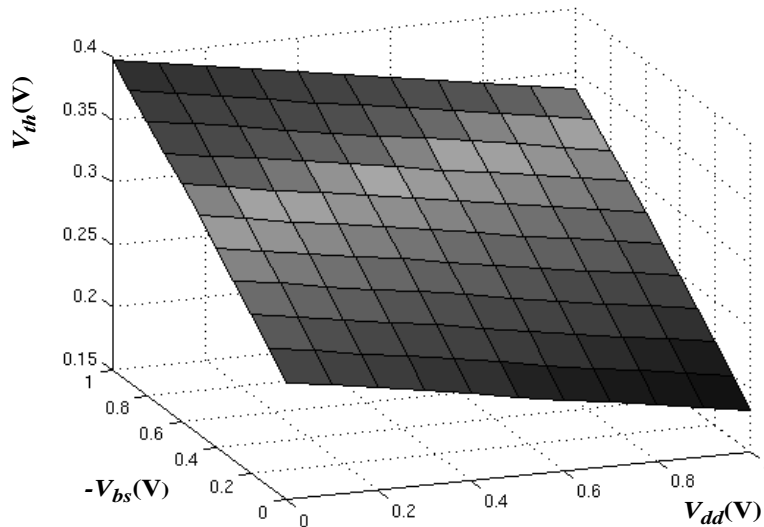


Figure 1. V_{th} vs. both V_{dd} and V_{bs} as generated by SPICE simulation for a deep-submicron process.

2.2 Power Consumption

The power consumed in a processor consists of three components as given by,

$$P = P_{AC} + P_{DC} + P_{SC} \quad (4)$$

where P_{AC} is the dynamic power, P_{DC} is the static power due to leakage, and P_{SC} is the negligible power due to short circuits when both PMOS and NMOS devices are on during signal transitions [14]. The dynamic power is given by,

$$P_{AC} = C_{eff} V_{dd}^2 f \quad (5)$$

where C_{eff} is the average switched capacitance per cycle, and f is the clock frequency. Figure 2 shows the major components of static current in a standard inverter. Although [15,16] consider only the leakage due to I_{subn} and I_{subp} , as [7,17] points out, the contributions of I_j and I_b can be significant. Thus, the static power consumption is given by,

$$P_{DC} \approx V_{dd} I_{subn} + |V_{bs}| (I_{jn} + I_{bn}) \quad (6)$$

where I_{subn} is the subthreshold leakage current, I_{jn} is the drain to body junction leakage current, and I_{bn} is the source to body junction leakage current through the NMOS device. Equation (6) is given for the inverter when its output state is high (i.e. the NMOS device is leaking). A similar equation can be derived for the inverter when the output state is low and the PMOS device is leaking.

The subthreshold leakage current through a transistor with $V_{ds}=V_{dd}$ and $V_{gs}=0$ is modeled by,

$$I_{subn} = \left(\frac{W}{L}\right) I_S \left[1 - e^{-\frac{V_{dd}}{V_T}} \right] e^{-\frac{(V_{th} + V_{off})}{n V_T}} \quad (7)$$

where W and L are the device geometries, I_S , n , and V_{off} are empirically determined constants for a given process, and V_T is the thermal voltage [11]. Since V_{off} is typically small and $1 - \exp(-V_{dd}/V_T)$ is nearly 1 for all V_{dd} , (7) can be approximated as,

$$I_{subn} = K_3 e^{-K_4 V_{th}} \quad (8)$$

where K_3 and K_4 are constant fitting parameters. Substitution of (3) into (8) yields,

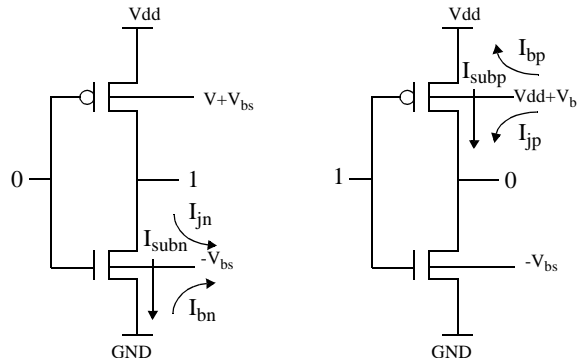


Figure 2. Static current sources for an inverter.

$$I_{subn} = K_3 e^{K_5 V_{dd}} e^{K_6 V_{bs}} \quad (9)$$

where K_5 and K_6 are constant fitting parameters. As $|V_{bs}|$ is increased, the current due to junction leakage, I_j , increases and counteracts the savings achieved by lowering I_{subn} . The maximum value of $|V_{bs}|$ before junction leakage overrides subthreshold current reduction is dependent on process and has been shown to vary from as high as -0.6V to -2.5V [8,18]. This crossover point is also highly dependent on temperature, where at higher operating temperatures, transistors exhibit a larger reduction in I_{subn} (and thus tolerate a larger $|V_{bs}|$) before I_j increases [8]. SPICE simulations for the 0.07 μ m process show that the crossover point is about -1.2V. Therefore, to be safe, V_{bs} was constrained between 0 and -1V, although in a different process, a lower cutoff point might be needed. I_j can be approximated as a constant,

$$I_{bn} + I_{jn} = I_j \quad (10)$$

and the total static current, I_{stat} , becomes,

$$I_{stat} = K_3 e^{K_5 V_{dd}} e^{K_6 V_{bs}} + I_j \quad (11)$$

Figure 3 is a SPICE generated plot of I_{stat} vs. simultaneous changes in V_{dd} and V_{bs} . A comparison between I_{stat} as generated by SPICE and I_{stat} as generated by (11) yields an average percent error of 2.09% and a maximum percent error of only 5.63% for $0.3 < V_{dd} < -1V$ and $-1 < V_{bs} < 0V$.

Substitution of (9) and (10) into (6) yields,

$$P_{DC} = V_{dd} K_3 e^{K_5 V_{dd}} e^{K_6 V_{bs}} + |V_{bs}| I_j \quad (12)$$

and finally,

$$= C_{eff} V_{dd}^2 f + V_{dd} K_3 e^{K_5 V_{dd}} e^{K_6 V_{bs}} + |V_{bs}| I_j \quad (13)$$

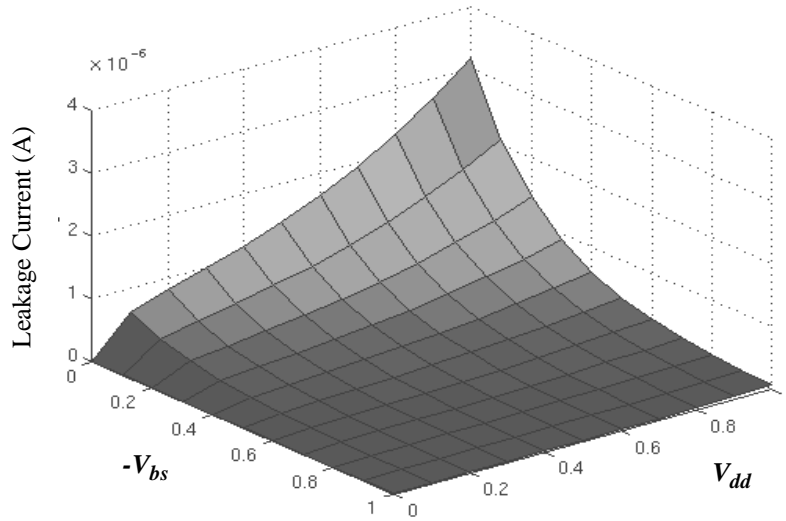


Figure 3. Leakage current through an NMOS device vs. V_{dd} and $-V_{bs}$ as generated by SPICE simulation.

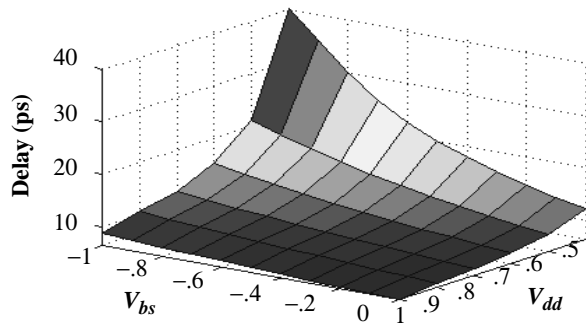


Figure 4. Circuit delay vs. V_{dd} and V_{bs} as generated by SPICE simulation.

2.3 Delay

The delay of a gate is a function of both the power supply and the threshold voltage of the internal transistors. Since the delay of complex gates remains proportional to the delay of a standard inverter, the circuit delay can be modeled similarly to the alpha-power model of an inverter [19,20] as,

$$t_{inv} = \frac{K_7}{(V_{dd} - V_{th})^\alpha} \quad (14)$$

where K_7 is a constant for a given process technology, and α is an indication of the amount of velocity saturation occurring in the device (α is typically 1.3-1.5 for short channel devices). The critical path delay in a circuit can be modeled as,

$$t_{crit} = L_d t_{inv} \quad (15)$$

where t_{crit} is the delay of the critical path and L_d is the so-called logic depth of the path [15]. Substitution of (3) and (14) into (15) yields,

$$f = \frac{((1 + K_1)V_{dd} + K_2V_{bs} - V_{th1})^\alpha}{L_d K_7} \quad (16)$$

Figure 4 shows the plot of delay vs. V_{dd} and V_{bs} as determined using SPICE. A comparison between the SPICE data and the operating frequencies calculated using (16) yields an average percent error of 9.8% and a maximum percent error of 33.2% for $0.5 < V_{dd} < 1V$, $-1 < V_{bs} < 0V$, and $\alpha=1$. While this maximum percent error is large, (16) produces worst-case frequencies which guarantee that the circuit will meet timing. The optimal power consumption, however, is not fully realized. Additionally, V_{dd} was limited to greater than 0.5V to ensure proper circuit operation and noise margins since the V_{th} of a transistor approaches 0.38 V when scaling.

3. Optimization

Now that the necessary models have been developed, the technique for finding optimal settings for implementing both DVS and ABB is presented. With three possible variables to control, V_{dd} , V_{bs} , and f , the optimization first begins with limiting the number of free variables.

3.1 Variable Reduction

The processor's algorithm for determining utilization based on workload generates a value for the required frequency eliminating one free variable. In order to eliminate a second variable, this frequency is treated as a constant for a given optimization point and (16) can be solved to find V_{dd} as a function of V_{bs} . If $\alpha = 1$ then (16) yields,

$$V_{dd} = \frac{L_d K_7 f - K_2 V_{bs} + V_{th1}}{1 + K_1} \quad (17)$$

which may be rewritten as,

$$V_{dd} = \begin{cases} K_8 V_{bs} + K_{f1} & \text{if } V_{dd} > 0.5 \\ 0.5 & \text{otherwise} \end{cases} \quad (18)$$

where, for a given frequency,

$$K_8 = \frac{-K_2}{1 + K_1}, \quad K_{f1} = \frac{V_{th1} + L_d K_7 f}{1 + K_1} \quad (19)$$

This leaves V_{bs} as the only free variable.

3.2 Energy Minimization

The energy consumed per cycle is defined as,

$$E_{cyc} = P f^{-1} \quad (20)$$

By substituting in (13), the total energy consumed per cycle for an entire circuit is given by,

$$E_{cyc} = C_{eff} V_{dd}^2 + L_g f^{-1} (V_{dd} K_3 e^{K_5 V_{dd}} e^{K_6 V_{bs}} + |V_{bs}| I_j) \quad (21)$$

where L_g is the number of logic gates in the circuit. Unfortunately, there is also energy required in switching the circuit between varying power modes. This switching energy, E_s , is given by,

$$E_s = |\Delta V_{dd}|^2 C_r + |\Delta V_{bs}|^2 C_s \quad (22)$$

where ΔV_{dd} is the change in V_{dd} , ΔV_{bs} is the change in V_{bs} , C_r is the capacitance of the power rail, and C_s is the total capacitance of the substrate and wells of the device. Let t be the duration of time in a given power mode then the total energy consumed in a particular mode is given by,

$$E_{tot} = E_s + t \cdot f \cdot E_{cyc} \quad (23)$$

Differentiating (23) with respect to V_{bs} yields,

$$\frac{\partial E_{tot}}{\partial V_{bs}} = \frac{\partial E_s}{\partial V_{bs}} + (t \cdot f) \frac{\partial E_{cyc}}{\partial V_{bs}} \quad (24)$$

where by substituting in (18),

$$\frac{\partial E_s}{\partial V_{bs}} = \begin{cases} 2(K_8^2 C_r + C_s)V_{bs} + 2C_r K_8(K_{f1} + V_{dd0}) \\ -2C_s V_{bs0} & \text{if } V_{dd} > 0.5 \\ -2C_s(V_{bs0} - V_{bs}) & \text{otherwise} \end{cases} \quad (25)$$

and

$$\frac{\partial E_{cyc}}{\partial V_{bs}} = \begin{cases} L_g K_3 f^{-1} (k_1 V_{bs} + k_2) e^{k_3 V_{bs} + k_4} - I_j L_g f^{-1} \\ + 2C_{eff} (k_5 V_{bs} + k_6) & \text{if } V_{dd} > 0.5 \\ \frac{L_g}{2f} (K_3 K_6 e^{K_6 V_{bs} + 0.5 K_5} - 2I_j) & \text{otherwise} \end{cases} \quad (26)$$

In (26), k_1 - k_6 are constants derived from the other process variables, K_1 - K_8 . Their values for a 10 inverter chain are presented in Table 1. Figure 5 shows the derivative of total energy vs. V_{bs} . The zero crossing indicates the V_{bs} for minimum energy consumption. Figure 6 shows the optimal V_{bs} and V_{dd} for minimum energy consumption for different required frequency, given a $50\mu\text{s}$ duration of operation. For any duration $t > 50\mu\text{s}$, the V_{dd} and V_{bs} values are independent of t while for a duration $t < 50\mu\text{s}$, V_{dd} and V_{bs} scale with t . The shorter duration cycles do not lend themselves to large voltage changes because the energy required to switch V_{dd} and V_{bs} can not be amortized over as many cycles as during the longer duration cycles. Figure 7 shows the energy savings achievable by using both DVS and ABB. The average energy reduction over all frequencies by simultaneous DVS and ABB as opposed to just DVS is 54% while the savings over a circuit with no scaling is 74%. SPICE simulated values for total energy and the expected values based on (23) agree with an average percent error of 12.7% and a maximum percent error of 28.8%.

Variable	Value	Variable	Value	Variable	Value
K_1	0.063	K_7	5.26×10^{-12}	V_{th1}	0.244
K_2	0.153	K_8	-0.144	I_j	4.80×10^{-10}
K_3	5.38×10^{-7}	t	5×10^{-5}	C_{eff}	2.00×10^{-15}
K_5	1.83	V_{dd0}	1	L_d, L_g	10
K_6	4.19	V_{bs0}	0	C_r	1×10^{-12}
$Max f$	15.6 GHz	C_s	1×10^{-12}		

TABLE 1. Constants for a $0.07\mu\text{m}$, 10 inverter chain.

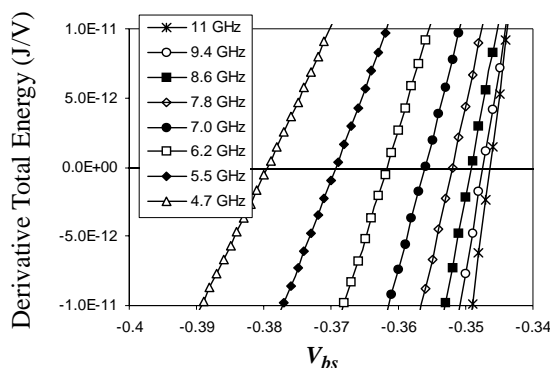


Figure 5. Derivative of total energy w.r.t. V_{bs} vs. V_{bs} . Zero crossing shows the V_{bs} value that produces minimum energy consumption for a given frequency.

4. Microprocessor Results

The proposed method of simultaneous DVS and ABB was applied to a mobile processor using the derived optimal trade-off between supply voltage and body-bias. The dynamic processor load was obtained through hardware monitoring as explained in the following section. The application of the simultaneous DVS and ABB method and the resulting energy savings are discussed in Sections 4.2 and 4.3.

4.1 Workload

Performance-setting algorithms dynamically adjust the processor's performance level while ensuring that the software running on the processor meets its deadlines. For some applications, there is a very clear notion of what these deadlines are. During video playback, for example, the performance-setting algorithm must ensure that the desired framerate (usually 30 frames/second) is achieved. Setting the performance too low would cause the application to not be able to decode and not display frames at the proper time, causing jerkier playback. Decoding a frame too soon, on the other hand, unnecessarily increases power consumption since finishing a task before its deadline implies that the performance level was set too high. The goal of the performance-setting strategy is to stretch the execution of each task exactly to its deadline and scale the supply voltage and body bias voltage to their optimal values for the required performance. The only difficulty is in knowing exactly what the deadlines are. Our algorithm is implemented in the Linux kernel and relies on monitoring system calls and inter-

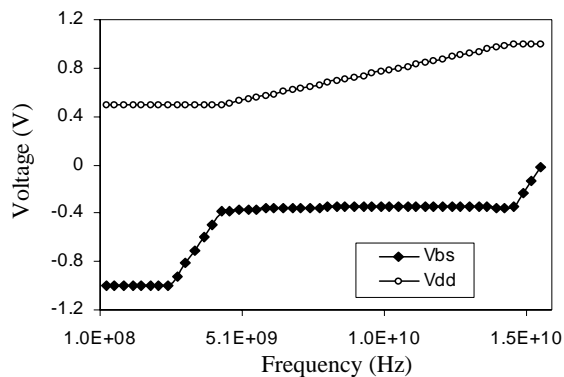


Figure 6. Plot of the V_{dd} and V_{bs} values for optimal energy reduction in a 50 μ s duration low-power state.

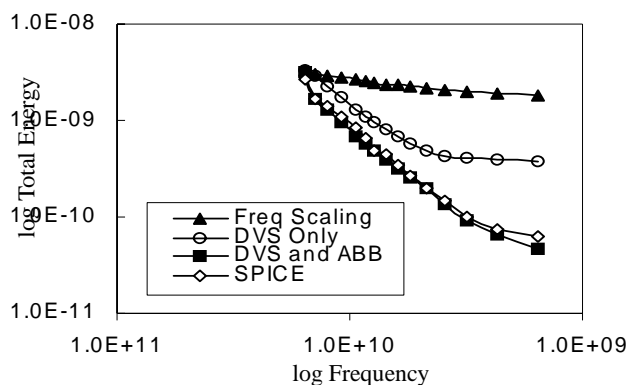


Figure 7. Total energy consumed by 10 inverters using low power scaling techniques for a 10ms time period.

task communication to derive deadlines automatically and without modification of user programs [2]. Unlike many similar algorithms, ours is equally effective for interactive and real-time (periodic) workloads.

The traces for this paper were collected on a Sony Picturebook PCG-C1VN which uses the Transmeta Crusoe 5600 processor whose performance level can be varied between 300 - 600MHz in 100MHz steps (or frequency scaled between 50 - 100% in 16% steps). While this processor has its own algorithm for controlling the processor performance levels, we have overridden it with our own performance-setting algorithm. During the benchmark runs, the processor's frequency was varied between 300MHz and 600MHz and the measured performance levels were used to compute the expected energy using either DVS alone or using simultaneous DVS and ABB. Moreover, we noticed that for many of our benchmarks, even the minimum speed of this processor was unnecessarily fast. Some of our applications would meet their deadlines with a performance level of 10% of peak. Therefore, we also estimated the effects on energy consumption for a conceptual processor that could run over a wider range of frequency values. The frequency values ranged from 10 - 100% in 5% steps. We compare these energy results with those from the more restricted range where the minimum frequency was restricted to 50% of maximum performance. The four benchmarks in this paper are:

- xmms-mp3: mp3 audio playback using the xmms player, which includes visual effects (See Figure 8).
- mpeg: video playback of Red's Nightmare.
- emacs: record of an editing session in emacs.
- os: record of user doing miscellaneous UNIX operations (e.g. grep, ls, vi, find, awk, perl, etc.).

4.2 Optimization

The constant values for the Crusoe processor were calculated using published data on the processor [21]. Since, the processor is fabricated in a 0.18 μ m process, the fitting parameters were adapted from the Berkeley predicted models for a 0.18 μ m process [13]. Table 2 shows the constants for the Crusoe processor in 0.18 μ m technology. It is recognized that as technology continues to scale, processes incur higher leakage [22]. In fact, the static power in current 0.18 μ m high-performance processors comprises 20% of total power [4]. Conservatively, our 0.18 μ m simulations have only 10% leakage power. To forecast for future generations, constant values were also calculated for the higher-leakage 0.07 μ m predicted process. The 0.07 μ m process's leakage power is 30% of

Variable	Value	Variable	Value	Variable	Value
K_1	0.053	K_7	51×10^{-12}	V_{th1}	0.359
K_2	0.140	K_8	-0.132	I_j	2.40×10^{-10}
K_3	3.0×10^{-9}	t	5×10^{-5}	C_{eff}	1.11×10^{-9}
K_5	1.63	V_{dd0}	1.6	L_d	37
K_6	3.65	V_{bs0}	0	C_r	1×10^{-6}
$Maxf$	600 MHz	C_s	4×10^{-6}	L_g	4×10^6

TABLE 2. Constants for the Crusoe 5600 processor in the 0.18 μ m process.

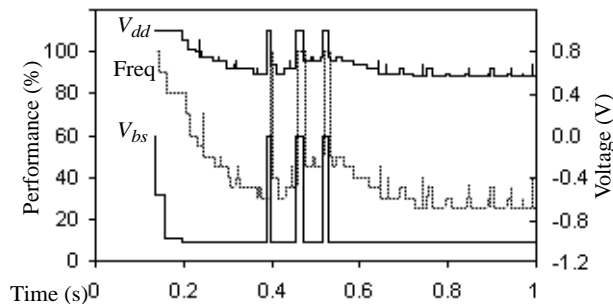


Figure 8. Subset of the trace for the xmms-mp3 player showing performance and optimal V_{dd} and V_{bs} .

dynamic power. To ensure a fair comparison, both the 0.18 μ m and 0.07 μ m processes had the ability to scale V_{dd} by up to 0.5V and V_{bs} by up to -1V. The minimum duration at any utilization was set at 200 μ s which is a conservative estimate of V_{dd} and V_{bs} switching times based on previous published data [6]. During these switching periods, the higher-power state was used as an estimate of total energy. Figure 8 shows a sub-section of the trace for the xmms-mp3 player and the required V_{dd} and V_{bs} values for energy optimization in the 0.07 μ m technology.

4.3 Energy Savings

Table 3 shows the energy reduction achieved by employing both DVS and ABB in the 0.18 μ m process using scaling between 50 - 100% in 16% steps. The values are shown for the four different workloads. In the 0.18 μ m process the average energy savings over DVS only schemes is 23%. The more aggressive performance scaling (10 - 100% scaling) does not yield any benefits in the 0.18 μ m process because the longer run times during active cycles override the benefits achieved during the idle states when the clock is halted and only static power is consumed. This is due to the relatively low-leakage nature of the 0.18 μ m process (10% of total power).

0.18 μ m Process	xmms-mp3	mpeg	emacs	os
No scaling	23 J	47 J	13 J	37 J
DVS alone (reduction vs. no scaling)	9.4 J (60%)	21 J (55%)	4.7 J (63%)	18 J (51%)
DVS & ABB (reduction vs. DVS alone)	7.6 J (19%)	19 J (10%)	2.8 J (40%)	14 J (21%)

TABLE 3. Energy consumed and percent reduction in the 0.18 μ m technology under several workloads with frequency scaling between 50 - 100% with 16% steps.

0.07 μ m Process	Freq. scaling between 50-100% in 16% steps				Freq. scaling between 10-100% in 5% steps			
	xmms-mp3	mpeg	emacs	os	xmms-mp3	mpeg	emacs	os
No scaling	65J	111J	50J	119J	65J	111J	50J	119J
DVS alone (reduction vs.no scaling)	26J (60%)	47J (57%)	18J (64%)	53J (55%)	15J (76%)	42J (62%)	11J (78%)	37J (70%)
DVS & ABB (reduction vs. DVS)	16J (38%)	36J (22%)	9.3J (48%)	34J (35%)	8.4J (45%)	32 (22%)	2.1J (80%)	19J (47%)

TABLE 4. Energy consumed and percent reduction by no scaling, DVS only, and DVS and ABB under several workloads with two frequency scaling regimes.

Table 4 shows the energy reduction achieved by simultaneous DVS and ABB scaling in the 0.07 μ m process. The performance scaling between 50 - 100% of peak shows an average energy reduction of 39% over DVS alone while the scaling between 10 - 100% of peak has an average energy reduction of 48%. The most benefit is achieved in applications like emacs where the processor spends a lot of time idling and consumes mostly static power. This static power is reduced by the body biasing.

5. Conclusion

We examined an energy reduction technique through simultaneous implementation of DVS and ABB and presented an analytical expression for power consumption and processor performance as functions of three control parameters (frequency, supply voltage, and body bias voltage). A closed-form method for finding the proper V_{dd} and V_{bs} for optimal power consumption was also presented. Furthermore, this optimal solution was easily obtained using process parameters from SPICE simulation and design specifications. The optimal parameters were applied to both actual and simulated workloads for a 600MHz, 0.18 μ m mobile processor. The results show that the simultaneous implementation of DVS and ABB power scaling techniques produce an average energy reduction of 23% in a 0.18 μ m process and 39% in a predicted 0.07 μ m process over DVS alone when scaling performance between 50 - 100%. Energy reductions of nearly 50% were achieved through more aggressive performance scaling (10 - 100%) in the 0.07 μ m process. The results also suggest that as technology scales and leakage power increases, simultaneous DVS and ABB scaling will become more effective.

References

- [1] T. D. Burd, T.A. Pering, et. al., "A dynamic voltage scaled microprocessor system," *IEEE J. Solid-State Circuits*, vol. 35, pp. 1571-1580, Nov. 2000.
- [2] K. Flautner, S. Reinhardt, T. Mudge, "Automatic performance setting for dynamic voltage scaling," *7th Intl. Conf. on Mobile Computing and Networking*, Rome, Italy, 2001.
- [3] L. Geppert, T.S. Perry, "Transmeta's magic show," *IEEE Spectrum*, vol. 37, pp. 26-33, May 2000.
- [4] <http://developer.intel.com/design/mobile/datashts/>
- [5] A. Chandrakasan, W. Bowhill, F. Fox eds., *Design of High-Performance Microprocessor Circuits*. Piscataway, NJ: IEEE Press, 2001.

- [6] H. Mizuno, K. Ishibashi, T. Shimura, T. Hattori, S. Narita, K. Shiozawa, S. Ikeda, K. Uchiyama, "A 18uA- Standby-Current 1.8V 200MHz Microprocessor with Self Substrate-Biased Data-Retention Mode," *Proc. IEEE International Solid-State Circuits Conference*, pp.280-281, 1999.
- [7] A. Keshavarzi, S. Narendra, et. al., "Effectiveness of reverse body bias for leakage control in scaled dual Vt CMOS ICs," *Intl. Symp. on Low Power Electronics and Design*, 2001.
- [8] X. Liu, S. Mourad, "Performance of submicron CMOS devices and gates with substrate biasing," *IEEE Intl. Symp. Circuits and Systems*, Geneva, Switzerland, May 28-31.
- [9] M. Miyazaki, J. Kao, A. Chandrakasan, "A 175mV Multiply-Accumulate Unit using an Adaptive Supply Voltage and Body Bias Architecture," *IEEE Intl. Solid-State Circuits Conf.*, pp.58-59, 2002.
- [10] S. Narendra, M. Haycock, et. al., "1.1V 1GHz Communications router with On-Chip Body Bias in 150nm CMOS," *IEEE Int. Solid-State Circuits Conf*, pp. 270-271, 2002.
- [11] P. Ko, J. Huang, et. al., "BSIM3 for Analog and Digital Circuit Simulation," *Proc. IEEE Symposium on VLSI Technology CAD*, pp. 400-429, Jan. 1993.
- [12] Z.H. Liu, C. Hu, J.H. Huang, et. al., "Threshold voltage model for deep-submicrometer MOSFETs," *IEEE Tran. Electron Devices*, vol. 40, pp. 86-95, 1993.
- [13] <http://www-device.eecs.berkeley.edu/~ptm/introduction.html>
- [14] H. Veendrick, "Short-circuit dissipation of static CMOS circuitry and its impact on the design of buffer circuits," *IEEE J. Solid-State Circuits*, vol. 19, pp. 468-473, Aug. 1984.
- [15] R. Gonzalez, et.al., "Supply and Threshold Voltage Scaling for Low Power CMOS," *IEEE J. Solid-State Circuits*, vol. 32, pp. 1210-1216, Aug. 1997.
- [16] M.R. Stan, "Optimal Voltages and Sizing for Low Power," *Intl. VLSI Design Conf.*, Goa, India, Jan. 1999.
- [17] M. Chen, H. Huang, et. al., "Back-gate bias enhanced band-to-band tunneling leakage in scaled MOSFETS," *IEEE Electron Device Letters*, vol. 19, no. 4, pp. 134-136, Apr. 1998.
- [18] A. Kesharvarzi, S. Narendra, et. al., "Technology scaling behavior of optimum reverse body bias for standby leakage power reduction in CMOS ICs," *Intl. Symp. on Low Power Electronics and Design*, pp. 252-254, 1999.
- [19] T. Sakurai, A.R. Newton, "Alpha-power law MOSFET model and its applications to CMOS inverter," *IEEE J. Solid-State Circuits*, vol. 25, no. 2, pp. 584-594, Apr. 1990.
- [20] K.A. Bowman, B.L. Austin, et. al., "A physical alpha-power law MOSFET model," *IEEE J. Solid-State Circuits*, vol. 34, pp. 1410 -1414, Oct. 1999.
- [21] http://www.transmeta.com/pdf/specifications/productbrief_tm5600_02aug00.pdf
- [22] S. Thompson, P. Packan, and M. Bohr, "MOS Scaling: Transistor Challenges for the 21st Century." *Intel Technology Journal*, Q3 1998.